Shear Forces, Root Rotations, Phase Angles and Delamination of Layered Materials

M. D. Thouless
Department of Mechanical Engineering
Department of Materials Science & Engineering
University of Michigan, Ann Arbor, MI 48109, USA

Abstract

In this paper, the concepts of root rotations and phase angles in laminated structures are reviewed, with particular reference to how the presence of a shear force affects the fracture mechanics of an interface. It is shown that it is possible to combine all the effects of shear into an effective root rotation, rather than the usual approach of invoking root rotation as a correction to a clamped Timoshenko beam. This simplifies the mechanics of the phenomenon, as root rotation is a general concept for interface cracks, and is not unique to shear loading. The root rotations enter into expressions for the energy-release rate associated with shear, and give rise to the crack-tip phase angles that provide a measure of how other modes of loading interact with shear loading. Additionally, the present analysis identifies the concept of a root displacement as an additional measure of the deformation at a crack tip. This is required to provide consistency with compliance-based approaches to the fracture mechanics of a double-cantilever beam, and allows one to make a direct connection to classical elastic-foundation models of that geometry.

February 2, 2018

Keywords: root rotation, shear loading, phase angles, laminated geometries, double-cantilever beam, energy-release rate

1 Introduction

The complications associated with transverse shear forces applied to layered materials have long been recognized, particularly with regard to the double-cantilever beam (DCB) geometry [1, 2, 3]. Conversely, the fracture mechanics for loading by pure moments is very straight-forward: the energy-release rate, $\mathcal{G}$, is dependent only on the applied moments, the elastic properties of the arms, and the thickness of the arms. The energy-release rate, along with the equivalent J-integral, and the corresponding work done against the cohesive tractions at the crack-tip, $\mathcal{W}_o$, are not dependent on the nature of the cohesive law for the interface. Experimental approaches have been developed to evaluate interfaces using this concept, with test configurations being designed to ensure loading by pure moments [4, 5]. However, more commonly, interfacial properties are measured using a DCB loaded by transverse forces [6, 7], so that the crack tip experiences both a moment and a shear force. This introduces the need to consider how shear may affect the interface mechanics.

Historically, shear loading has generally been considered to have two distinct effects in a DCB geometry [1]. First, shear results in an additional contribution to the compliance of the arms themselves. The complications associated with the analysis of this effect have been described by Barber [8] as a problem of satisfying all the conditions at a clamped boundary. Second, the arms of a DCB can rotate at the crack tip, since they are not clamped rigidly. This crack-tip rotation is termed *root rotation*. One contribution to root rotation arises even in perfectly bonded systems,[1] because the elastic arms are compliant beyond the crack tip. A second contribution

[1]The term "perfect bonding" is used here to describe an interface having a traction-separation law with an infinitely steep loading slope, corresponding to a cohesive length of zero [9]. Any compliance associated with the traction-separation law results in a finite cohesive length [9].

arises if the bonding along the interface results in additional compliance.

As an illustration of the effects of shear, consider the displacement of a point force (per unit width), P_∞, located at a distance a_o from the crack tip in a symmetrical, perfectly bonded, linear-elastic double-cantilever beam whose arms have a Young's modulus of E, shear modulus of G, and thickness of h (Fig. 1). The displacement of the force on each arm is given by [1]

$$\Delta = \frac{4P_\infty a_o^3}{Eh^3} + \frac{P_\infty a_o}{\kappa_s G h} + a_o\varphi \ , \tag{1}$$

where κ_s is the shear coefficient, which is often taken to be 5/6, and φ is the root rotation. In this expression, the first term is the result assuming an Euler-Bernoulli beam, the second term is the shear correction for a clamped Timoshenko beam, and the third term represents the root-rotation correction.

Calculating the displacement from Eqn. 1 then becomes a matter of determining φ as a function of geometry and loads. Once the displacement is known, the potential energy of the arms can be determined, from which $\mathcal{G}$ can be calculated. Early work used approximate assumptions to model the deformation at the crack tip. These gave results that, while usefully accurate, were not rigorously correct. For example, Gillis and Gilman [1] assumed a simple power-law (quadratic) dependence between φ and the crack length. Mostovoy *et al.* [2] assumed that the effect of root rotation could be modelled by changing the effective crack length. The notion of an effective crack length was further refined [10], and forms the basis of current standards for DCB tests [6, 11].[2] More formally, magnitudes of the root rotations have been determined

[2]The ASTM standard for adhesive bonding [7] uses the basic results of Mostovoy *et al.* [2], with their approximation that $\kappa = 2/3$ and $\nu = 1/3$, but with no suggested modification for root-rotation effects.

numerically [12], and from approximate analytical analyses [13, 14]. The corrections associated with root rotations have also been determined empirically for specific test geometries [15, 16].

An alternative approach for calculating the effect of shear in laminated geometries has been provided by Li *et al.* [17] for linear systems. In this approach, any general loading is expressed as the superposition of four fundamental crack-tip geometries shown in Fig. 2. These consist of crack-tip (a) axial forces and (b) bending moments that were analyzed by Suo and Hutchinson [18], plus crack-tip (c) symmetrical and (d) unsymmetrical transverse forces that were analyzed by Li *et al.* [17]. Each of these four fundamental geometries gives a crack-length-independent expression for the energy-release rate, and a corresponding phase angle. The phase angle, which is defined more formally in a subsequent section, is the parameter that allows one to combine the results for each fundamental geometry to solve any general problem [17]. In a very insightful paper, Andrews and Massabò [12] showed how to link this approach of energy-release rates and phase angles to the concept of root-rotations. They showed how root-rotations contribute to the energy-release rates associated with the two types of shear, and to the phase angles that allow these energy-release rates to be combined with the other crack-tip solutions.

Generally, analyses of root-rotations for perfectly bonded systems have followed Eqn. 1 in separating the effect of shear into two parts: (i) a shear correction to the deformation of a clamped beam, following the Timoshenko analysis, and (ii) a crack-tip rotation to correct for the first assumption of a clamped boundary. In this present paper, we show that one can replace these two effects by a single, effective rotation at the crack tip. This may be a simpler way of visualizing the mechanics, and

simple-beam theory can be used to model the system since all the effects of shear are included in the root rotation applied to the boundary condition for the beam analysis.

The approach proposed in this paper is illustrated by the schematic diagram of Fig. 3. This figure shows how the centroidal axis of the section rotates at the tip of an interface crack, coupling both the effects of shear and root rotation. The usual approach of imposing a rotation on the clamped boundary of a Timoshenko beam would result in a kink in the angle at the crack tip, whereas, the smooth slope assumed here must also be accompanied by a root-displacement, u_{o_A}, which is discussed in a subsequent section. This root displacement has one contribution from the separation of the interface, δ_{o_A}, and a second contribution from the elastic deformation of the arms. It should be emphasized that the results we obtain from this combined approach are no different from those obtained by Andrews and Massabò [12]. Whether one splits the effects of shear into two parts, or combines them, has no effect on any of the solutions for phase angles or energy-release rates. It only affects the value of what one defines as 'root rotation'. However, assuming a clamped boundary, using the Timoshenko analysis to account for shear effects in a clamped beam, and then rotating the boundary to correct for the original assumption of a clamped boundary, may seem to be arbitrarily complicated compared to the present approach.

It should be emphasized that neither the present approach, nor the approach based on a clamped and rotated boundary, capture the full details of the displacement fields along the length of the arms. Both merely capture the essential aspects required to analyze the fracture mechanics. From this perspective, it does not matter whether the gradient of the centroidal axis of the section is smooth in the region of the crack tip, as in the present analysis, or whether there is a kink, as is implicit for a root-

rotation correction to a Timoshenko beam. Nor do the details of the deformation of the sections along the beam matter. Any additional information that might arise from a full elasticity analysis has no influence on the fracture mechanics, and can be neglected without loss of rigor.

There is, however, one concept that the present approach identifies, which is not apparent from an analysis based on the rotation of a clamped beam. It can be seen from the schematic diagram of Fig. 3 that the smooth slope of the centroidal axis (rather than the implied kink of a corrected Timoshenko beam) indicates that there must also be a root displacement, u_{o_A}, at the crack tip. As discussed in a later section of the paper, this root displacement affects the compliance of a DCB, and is required for consistency with a compliance-based analysis of the energy-release rate. Furthermore, such a root displacement needs to be included in analyses of the wedge test (a DCB geometry loaded by insertion of a wedge into the crack mouth).

2 Analytical background

2.1 Interfacial fracture mechanics

In this paper we use results of interfacial mechanics recast from the perspective of a cohesive-zone approach to fracture, involving normal and shear tractions across the interface. Within this framework, concepts such as the energy-release rate, $\mathcal{G}_o$, and the crack-tip phase angle, ψ_o can be expressed in terms of the work done against the tractions at the crack tip. It should be noted that, from a cohesive-zone perspective, linear-elastic fracture mechanics (LEFM) can be viewed as a perfectly-bonded, limiting condition, corresponding to a cohesive-length scale of zero [9], in which the

interface has no thickness, and plots of the mode-I and mode-II tractions against displacement are represented by delta functions with total areas equal to the corresponding values of toughness. This formulation is consistent with the LEFM assumptions of an infinite interfacial strength and an energy-based fracture criterion.

The value of the J-integral, J_{ext}, taken along a contour connecting points on the two traction-free surfaces of a crack is equal to the energy-release rate $\mathcal{G}_o$:

$$J_{ext} = -\frac{\partial \Pi}{\partial a_o} = \mathcal{G}_o \ , \tag{2}$$

where a_o is the length of the traction-free crack, and Π is the potential energy (per unit width) of the elastic arms, excluding any work done against the cohesive tractions ahead of the crack tip. The value of the J-integral taken on a local contour along the two bonded portions of the interface, J_{loc}, is equal to $\mathcal{W}_o$, which is the sum of the work done against the normal and shear tractions at the crack tip, $\mathcal{W}_{I_o}$ and $\mathcal{W}_{II_o}$, respectively. More formally,

$$J_{loc} = \mathcal{W}_o = \mathcal{W}_{I_o} + \mathcal{W}_{II_o} = \int_0^{\delta_{n_o}} \sigma_n d\delta_n + \int_0^{\delta_{s_o}} \tau_s d\delta_s \ , \tag{3}$$

where σ_n and τ_s are the normal and shear tractions, δ_n and δ_s are the relative normal and shear displacements across the interface, and the subscript 'o' indicates the value at the cohesive crack tip. By virtue of the path-independence of the J-integral, we know that $J_{ext} = J_{loc}$, so that $\mathcal{G}_o = \mathcal{W}_o$. However, it should be noted that the energy-release rate is a scalar quantity, whereas the work done against the crack-tip tractions can be decomposed into the two orthogonal components of mode-I and mode-II.

The two orthogonal components of the work done against crack-tip tractions can be used to define the crack-tip phase angle [9, 19, 20]:

$$\psi_o = \tan^{-1} \sqrt{(\mathcal{W}_{II_o}/\mathcal{W}_{I_o})} \ . \tag{4}$$

This definition provides a general expression of how energy is partitioned at the crack tip, and its form has been chosen to make it immediately equivalent to the conventional definition of a phase angle in LEFM, for which the two components of work done against crack-tip tractions are proportional to the square of the stress-intensity factors. This definition of the phase angle has been shown to give the results predicted by LEFM in cohesive-zone models with relatively small cohesive-length scales [9, 19, 20]. This definition also addresses the well-known conundrum of how to describe mixed-mode conditions for bimaterial problems [19, 20].

Although the phase angle is commonly associated with its role in describing the partition of energy at the crack tip, it has another important role in the superposition of solutions for different loading conditions. If the system is linear (this includes systems with linear traction-separation laws, or with small cohesive-length scales), the work done against crack-tip tractions can be added according to the cosine law [17].[3] For example, if one set of loads gives rise to crack-tip work, $\mathcal{W}_o^a$, with a phase angle, ψ_o^a, and a second set of loads gives rise to crack-tip work, $\mathcal{W}_o^b$, with a phase angle, ψ_o^b, the work done against crack-tip tractions for the combined loading is given by

$$\mathcal{W}_o = \mathcal{W}_o^a + \mathcal{W}_o^b + 2\sqrt{\mathcal{W}_o^a \mathcal{W}_o^b}\cos(\psi_o^a - \psi_o^b) \; . \tag{5}$$

Given the equivalency between $\mathcal{G}_o$ and $\mathcal{W}_o$, energy-release rates can be added in a similar fashion:

$$\mathcal{G}_o = \mathcal{G}_o^a + \mathcal{G}_o^b + 2\sqrt{\mathcal{G}_o^a \mathcal{G}_o^b}\cos(\psi_o^a - \psi_o^b) \; . \tag{6}$$

[3]For a linear system, the work done against the tractions is proportional to the square of the loads. Therefore, if the crack-tip work is split into orthogonal components, the square roots of these components can be summed. Hence, the cosine law that is cited.

2.2 Fracture of layered materials

The analyses in this paper are performed for bilayers in which the top beam (or layer) has a modulus of $\bar{E}_A$ and a thickness of h_A, and the bottom beam (or layer) has a modulus of $\bar{E}_B$ and a thickness of h_B. Without any loss of generality, the beams can be assumed to be either isotropic or orthotropic. For an isotropic beam, $\bar{E} = E$ in plane stress, and $\bar{E} = E/(1-\nu^2)$ in plane strain, where ν is Poisson's ratio. For an orthotropic beam, $\bar{E} = E_{11}$ in plane stress, and $\bar{E} = E_{11}/(1-\nu_{13}\nu_{31})$ in plane strain [16], where the axis x_1 is aligned with the direction of crack growth, the axis x_2 is perpendicular to the plane of the interface, and the axis x_3 is the orthogonal direction.

As discussed in Section 1, any general loading of a laminated structure can be reduced to a set of four basic loads acting at the tip of an interface crack (Fig. 2): axial forces, moments, symmetrical shear forces and non-symmetrical shear forces [17]. Separate results have been established for the energy-release rate (crack-tip work) and the phase angles for each of these four basic loads, and the results for general loading can be obtained by superposition [17], as described above.

If an interface crack is loaded only by crack-tip moments (Fig. 2a), M_o, the energy-release rate and, hence, the work done against the tractions at the crack-tip, is given by [18]:

$$\mathcal{G}_o^M = \mathcal{W}_o^M = \tilde{g}_m \frac{M_o^2}{\bar{E}_A h_A^3} \,, \tag{7}$$

where

$$\tilde{g}_m = 6\left(\tilde{\Sigma}\tilde{H}^3 + 1\right) \,,$$

$\tilde{H} = h_A/h_B$, and $\tilde{\Sigma} = \bar{E}_A/\bar{E}_B$. Alternatively, this equation can be expressed in terms

of the first Dundurs' parameter, $\tilde{\alpha}$, for isotropic materials: $\tilde{\alpha} = (\tilde{\Sigma} - 1)/(\tilde{\Sigma} + 1)$ [21], instead of the modulus ratio, $\tilde{\Sigma}$. The corresponding phase angle is ψ_o^M. The phase angle also depends on $\tilde{H}$ and $\tilde{\Sigma}$, but it has an additional dependency on the second Dundurs' parameter [21], $\tilde{\beta}$, and on the cohesive law.

If an interface crack is loaded by axial forces (Fig. 2b), N_o, the energy-release rate and, hence, the work done against the tractions at the crack-tip, is given by [18]:

$$\mathcal{G}_o^N = \mathcal{W}_o^N = \tilde{g}_n \frac{N_o^2}{\bar{E}_A h_A} \ , \tag{8}$$

where,

$$\tilde{g}_n = \left[0.5 + \tilde{\Sigma}\tilde{H}\left(1.5\tilde{H}^2 + 3\tilde{H} + 2\right)\right] \ .$$

The corresponding phase angle is ψ_o^N, which depends on $\tilde{H}$, $\tilde{\Sigma}$, $\tilde{\beta}$, and the cohesive law.

The energy-release rate for a combined loading of moments and axial forces is given by [22]

$$\mathcal{G}_o = \mathcal{W}_o = \tilde{g}_m \frac{M_o^2}{\bar{E}_A h_A^3} + \tilde{g}_n \frac{N_o^2}{\bar{E}_A h_A} + 6\left(1 + \tilde{H}\right)\tilde{\Sigma}\tilde{H}^2 \frac{M_o N_o}{\bar{E}_A h_A^2} \ . \tag{9}$$

As shown in Ref. [17], this can be re-expressed in the form of Eqn. 6 as

$$\mathcal{G}_o = \mathcal{W}_o = \mathcal{G}_o^M + \mathcal{G}_o^N + 2\sqrt{\mathcal{G}_o^M \mathcal{G}_o^N}\cos(\psi_o^M - \psi_o^N) \ . \tag{10}$$

where

$$\cos(\psi_o^M - \psi_o^N) = \frac{3\left(1 + \tilde{H}\right)\tilde{\Sigma}\tilde{H}^2}{\tilde{g}_m \tilde{g}_n} \ . \tag{11}$$

It should be noted that, while ψ_o^M and ψ_o^N both depend on $\tilde{\beta}$ and the cohesive law, the difference between them does not.

Equations 7, 8 and 11 are always valid for any geometry, modulus mismatch and any form of cohesive law along the interface. The only requirements are that the beams must be linear elastic, and that the bonded ligament must be sufficiently long to ensure no interfacial displacements at the remote boundary far ahead of the cohesive crack tip. Furthermore, the actual values of the individual phase angles will depend on the details of the cohesive tractions only if the cohesive-length scale is relatively large, or if the normal and shear tractions across the interface are coupled (for example, if $\tilde{\beta} \neq 0$) [19, 20]. In particular, the crack-tip phase angle, ψ_o^M, has been computed for isotropic [18] and orthotropic [22] materials in the limit of a very small cohesive-length scale (LEFM) and uncoupled tractions.[4]

If the system is linear, the energy-release rate and the crack-tip work for a layered material loaded by a pair of symmetrical transverse shear forces, V_{o_d}, at the crack tip, is of the form [17]

$$\mathcal{G}_o^{V_d} = \mathcal{W}_o^{V_d} = \tilde{g}_d \frac{V_{o_d}^2}{\bar{E}_A h_A} \ , \tag{12}$$

In contrast to Eqns. 7 and 8 this equation is correct only in the special case of a linear system. Furthermore, unlike $\tilde{g}_m$ and $\tilde{g}_n$ that can be found rigorously from a simple energy-balance or J-integral, $\tilde{g}_d$, along with the corresponding phase angle, $\psi_o^{V_d}$, needs to be calculated numerically. These two parameters are both functions of $\tilde{\alpha}$, $\tilde{H}$ and $\tilde{\beta}$ for isotropic materials, and have been determined in the LEFM limit (with $\beta = 0$) [17]. They are functions of $\tilde{H}$ and the orthotropy ratios ($\tilde{\lambda} = \bar{E}_{22}/\bar{E}_{11}$, and $\tilde{\rho} = \sqrt{\bar{E}_{11}\bar{E}_{22}}/2G_{12} - \sqrt{\bar{\nu}_{12}\bar{\nu}_{21}}$, where $\bar{\nu} = \nu$ in plane stress and $\bar{\nu} = \nu/(1+\nu)$ in plane strain) for orthotropic materials [12], and can be deduced from the numerical

[4]Suo and Hutchinson [18] have also provided results for the phase angle with respect to an arbitrary geometrical length, for $\tilde{\beta} \neq 0$ and LEFM conditions. However, the relationship of this quantity to the actual value of ψ_o depends on the details of the cohesive law [19, 20], even when the cohesive-length scale is vanishingly small.

results given in Ref. [12] for the LEFM limit.

2.3 Additional results for the DCB geometry

The analysis in this paper is presented for the general asymmetrical double-cantilever beam (DCB) geometry shown in Fig. 4. The DCB is loaded by a general combination of applied moments, M_∞, and transverse forces, P_∞, at a distance a_o from the crack tip. There are two very powerful results for this geometry that are independent of the crack length, and are given by the values of the J-integral evaluated along a path on the external boundaries. These two results are rigorous and completely general, with no assumptions being made about the deformation of the beams or about the from of the cohesive tractions. They rely only on the ligament ahead of the crack tip being long enough to ensure that there are no displacements across the interface.

If the DCB is loaded only by applied forces, P_∞, the energy-release rate and work done against crack-tip tractions can be found from the J-integral as [23, 24, 25]

$$J_{ext} = P_\infty \left(\Theta_A + \Theta_B\right) = \mathcal{G}_o = \mathcal{W}_o \tag{13}$$

where Θ_A and Θ_B are the rotations at the loading points of the two arms, both being defined as positive if they rotate the end of each beam away from the interface. This sign convention is consistent with the positive directions of the moments, indicated in Fig. 2, and is used for all rotations in this paper.

A related result is the value of the J-integral evaluated along a path on the external boundaries of a DCB loaded simultaneously by a transverse force, P_∞, and a moment,

M_∞. Following a similar analysis to those done in Ref. [26],

$$J_{ext} = \frac{6M_\infty^2}{\bar{E}_A h_A^3}\left[\tilde{\Sigma}\tilde{H}^3 + 1\right] + P_\infty\left(\Theta_A + \Theta_B\right) = \mathcal{G}_o = \mathcal{W}_o\,. \tag{14}$$

The two rotations in this equation, Θ_A and Θ_B, are now dependent on both the applied moments and the applied transverse forces. It is important to appreciate that Eqns. 7 and 13 cannot be simply added together, since the rotations are affected by both P_∞ and M_∞. Furthermore, as with the previous equation, Eqn. 14 is a completely general and rigorous result that makes no assumption about the nature of the elastic deformation of the beams nor of the cohesive law. It relies only on the assumption of a sufficiently long ligament ahead of the crack to ensure vanishingly small interfacial displacements at the boundary.

3 Root rotations in double-cantilever beams

3.1 General calculations

If a DCB is loaded by a general combination of applied moments, M_∞, and transverse forces, P_∞, the work done against the tractions at the crack tip is given by the J-integral of Eqn. 14. The angles, Θ_A and Θ_B, have three components: (i) a contribution from beam bending in response to the applied moment, (ii) a contribution from beam bending is response to the applied load, and (iii) the root-rotation at the crack tip. Both the moment and the shear force acting at the crack tip contribute to the root rotation.

Using Euler-Bernoulli beam theory,[5] the two angles are given by,

$$\Theta_A = \frac{6P_\infty a_o^2}{\bar{E}_A h_A^3} + \frac{12M_\infty a_o}{\bar{E}_A h_A^3} + \theta_{o_A}$$
$$\Theta_B = \frac{6P_\infty a_o^2}{\bar{E}_B h_B^3} + \frac{12M_\infty a_o}{\bar{E}_B h_B^3} + \theta_{o_B} \ , \tag{15}$$

where θ_{o_A} and θ_{o_B} are the root rotations for the two arms. From the perspective of the crack tip, the loading condition is represented by a combination of the fundamental geometries shown in Fig. 2(b) and (c), with $M_o = M_\infty + P_\infty a_o$, and $V_{o_d} = P_\infty$. Equation 15 and these two expressions allow Eqn. 14 to be written in terms of the crack tip loads:

$$\mathcal{W}_o = V_{o_d}\theta_o + \frac{6M_o^2}{E_A h_A^3}\left[\tilde{\Sigma}\tilde{H}^3 + 1\right] \ , \tag{16}$$

where $\theta_o = \theta_{o_A} + \theta_{o_B}$ depends on the geometry, modulus mismatch, and the details of the cohesive law.

In the special case of $M_\infty = -P_\infty a_o$, there is a state of pure symmetrical shear at the crack tip, with $M_o = 0$. Equation 16 then shows that the work done against the tractions at the cohesive-crack tip is given by

$$\mathcal{W}_o^{V_d} = V_{o_d}\theta_o^{V_d} \ , \tag{17}$$

where $\theta_o^{V_d} = \theta_{o_A}^{V_d} + \theta_{o_B}^{V_d}$, and is the total root rotation associated with pure shear. This is a completely general result, subject only to the assumption that the arms of the DCB are linear elastic. It does not depend on the form of the cohesive law. In the subsequent sections of this paper, we will present values of $\theta_o^{V_d}$ corresponding to some special cases.

[5] As emphasized in Section 1, Timoshenko beam theory is not used, because the shear deformation of the beam is wrapped into the root rotation.

If the system is linear,[6] dimensional arguments can be used to show that the root-rotation must be given by

$$\theta_o^{V_d} = \tilde{\theta}_d V_{o_d} / \bar{E}_A h_A \ , \tag{18}$$

where $\tilde{\theta}_d$ is a constant that depends on the geometry, elastic properties and cohesive law. When Eqn. 18 is substituted into Eqn. 17, one obtains

$$\mathcal{W}_o^{V_d} = \tilde{\theta}_d \frac{V_{o_d}^2}{\bar{E}_A h_A} \ , \tag{19}$$

which is identical to Eqn. 12, with $\tilde{g}_d = \tilde{\theta}_d$. This confirms the equivalency of the approach proposed by Li *et al.* [17] and that proposed by Andrews and Massabò [12], with the calculation of a single parameter being needed in both approaches.

In a linear system, the root rotation arising from the crack-tip moment, θ_o^M, can be separated from that arising from the crack-tip shear, $\theta_o^{V_d}$, with the total root rotation being given as

$$\theta_o = \theta_o^{V_d} + \theta_o^M \ . \tag{20}$$

After substituting this equation into Eqn. 16, Eqns. 7 and 17 can be used to show that

$$\mathcal{W}_o = \mathcal{W}_o^{V_d} + \mathcal{W}_o^M + V_{o_d} \theta_o^M \ . \tag{21}$$

By comparing this to the general expression (Eqn. 5) for adding different contributions to the work done against crack-tip tractions, we can see that

$$\cos(\psi_o^M - \psi_o^{V_d}) = \frac{V_{o_d} \theta_o^M}{2\sqrt{\mathcal{W}_o^{V_d} \mathcal{W}_o^M}} \ . \tag{22}$$

[6] As stated earlier, a linear system is one for which the arms are linear, and the cohesive law is either linear or has a very small cohesive-length scale.

In other words, the root rotation induced by a moment plays a role in the relative phase angle between moment-loaded cracks and shear-loaded cracks [12].

In a linear system, the root rotation induced by a crack-tip moment, M_o, must be of the form:

$$\theta_o^M = \tilde{\theta}_m M_o / \bar{E}_A h_A^2 \,, \tag{23}$$

where $\tilde{\theta}_m$ is a constant that depends on the geometry, modulus mismatch across the interface and the details of the cohesive law. Therefore, Eqn. 22 can be expressed as

$$\cos\left(\psi_o^M - \psi_o^{V_d}\right) = \tilde{\theta}_m \left[24\tilde{\theta}_d(\tilde{\Sigma}\tilde{H}^3 + 1)\right]^{-1/2} \,. \tag{24}$$

Again, this confirms the equivalency of the approach proposed by Li *et al.* [17] and that proposed by Andrews and Massabò [12]. In both approaches, three numerical parameters are needed to completely describe the fracture mechanics (including the mode-mixedness of a particular geometry or combination of loads). One either needs to compute $\tilde{g}_d$ and two phase angles [17], or two root rotations and one phase angle [12].

3.2 LEFM values for root rotations

The results given in the previous section are generally valid for linear systems. In particular, the results are valid for both isotropic and orthotropic systems under LEFM conditions (with small cohesive-length scales). The two root-rotation coefficients, $\tilde{\theta}_d$ and $\tilde{\theta}_m$, can be deduced for isotropic systems from the energy-release-rate and phase-angle results of Li *et al.* [17]. In that paper, values for $\tilde{\theta}_d = \tilde{g}_d$ are given directly as the numerical constants associated with the energy-release rate. The values of $\tilde{\theta}_m$ can be computed from Eqn. 24, using the values of ψ_o^M and $\psi_o^{V_d}$ also provided Ref. [17].

These two coefficients are presented in Tables (1) and (2).

Andrews and Massabò [12] have shown that the coefficients are of the form

$$\tilde{\theta}_d = \tilde{\theta}_d^*(\tilde{H}, \tilde{\rho})\tilde{\lambda}^{-1/2}$$
$$\tilde{\theta}_m = \tilde{\theta}_m^*(\tilde{H}, \tilde{\rho})\tilde{\lambda}^{-1/4} \,, \tag{25}$$

for orthotropic systems. As noted earlier, the effects of shear in Ref. [12] are divided into a contribution associated with shear deformation of a clamped cantilever beam, plus a contribution in the form of a rotation that is associated with a correction to the assumption of a clamped boundary. Inspection of Ref. [12], and a comparison with the form of the root rotation given in the present paper, shows that $\tilde{\theta}_d^*$ can be computed using the equation

$$\tilde{\theta}_d^* = \left[\tilde{b}_d + (1+\tilde{H})\tilde{\rho}\kappa_s^{-1}\right] \,, \tag{26}$$

where $\tilde{b}_d$ is the difference between the two constants given in Table 1 of Ref. [12], and $\kappa_s = 5/6$. The parameter $\tilde{\theta}_m^*$ can be obtained directly from Ref. [12]. Summaries of the two coefficients obtained from the results of that paper are given in Tables 3 and 4.

A comparison between the results of Tables 1 and 2, and those of Tables 3 and 4 show only minor discrepancies in the special cases where they can be directly compared, and confirm the excellent agreement between the two sets of numerical calculations given in Refs. [12] and [17].

The results of this section can also be expressed in terms of energy-release rates and phase angles, rather than as root rotations. The phase angles, ψ_o^M and $\psi_o^{V_d}$, can be obtained directly from Ref. [17] for isotropic materials, and are not reproduced

here. Phase angles for orthotropic materials are independent of $\tilde{\lambda}$, and have only a weak dependence on $\tilde{\rho}$ [22]. Detailed results for values of ψ_o^M do not exist in the literature, since the dependence on $\tilde{\rho}$ is so weak that they are assumed to be given by the isotropic results [22]. Based on this assumption, Eqn. 24 and the appropriate values of $\tilde{\theta}_d$ and $\tilde{\theta}_m$ are used to compute the values of $\psi_o^{V_d}$ summarized in Table 5 for orthotropic materials.

4 Symmetrical double-cantilever beams

For the special case of $\tilde{\Sigma} = \tilde{H} = 1$, $\psi_o^M = \psi_o^{V_d} = 0$ (by symmetry). Equation. 6 can then be used to show that

$$\mathcal{W}_o = \left(\sqrt{\mathcal{W}_o^M} + \sqrt{\mathcal{W}_o^{V_d}} \right)^2 , \tag{27}$$

and Eqn. 24 gives $\tilde{\theta}_m = 4\sqrt{3\tilde{\theta}_d}$. Therefore, if only a transverse force of P_∞ is applied at a distance a_o from the crack tip, so that $M_o = P_\infty a_o$ and $V_{o_d} = P_\infty$, Eqns. 7, 19 and 27 can be used to show that the work done against the crack-tip tractions is

$$\mathcal{W}_o = \frac{12P_\infty^2}{\bar{E}h^3} \left(a_o + \sqrt{\frac{\tilde{\theta}_d}{12}} h \right)^2 = \mathcal{G}_o \, . \tag{28}$$

This result, with $\tilde{\theta}_d = 5.44$ (Table 1), is identical (within a numerical error corresponding to the third significant figure) to the equation for the energy-release rate for an isotropic, symmetrical DCB under LEFM conditions given in [17], and closely approximates other numerical results [15]. With $\tilde{\theta}_d = 5.44\tilde{\lambda}^{-1/2}$ being substituted into Eqn. 28, the general form for an orthotropic system with $\tilde{\rho} = 1$ is obtained [12, 27]. In particular, it is noted that the quantity $\tilde{\theta}_m^*/24$ is identically equal to the empirical correction factor $Y(\rho)$ described in Ref. [16] for $\tilde{H} = 1$.

The form of Eqn. 28 lends itself to the commonly quoted concept that the effect of root-rotation can be expressed in terms of an effective increase in the crack length [3, 25]. It can be seen from Eqn. 28 that this effective increase in crack length is given by $\sqrt{\tilde{\theta}_d/12}h$. This approach is of practical use because it is not limited to systems with small cohesive-length scales (the value of $\tilde{\theta}_d$, and the effective crack length, increase with cohesive-length scale). However, it should be emphasized that such a form manifests itself rigorously only in the special case of a symmetrical, linear system.

Table 1 shows that the effective increase in crack length for an isotropic, linear-elastic, symmetrical DCB is given by $a_e = 0.673h$, rather than the commonly quoted value of $0.64h$. The latter result is derived from Kanninen's elastic-foundation model [3], and is discussed in more detail in Section 4.2. This concept of an effective crack length can be adapted for orthotropic materials. For example, Williams [10] derives an approximate equation for the effective increase in the crack length using a combined analytical and numerically-based empirical approach. Expressed in terms of the orthotropy ratios used in the present paper, Williams' equation is given by [10]

$$a_e/h = \sqrt{\frac{2.36(\tilde{\rho}+0.3\tilde{\lambda}^{1/2})}{11}\left\{3-2\left[\frac{2.36(\tilde{\rho}+0.3\tilde{\lambda}^{1/2})}{1+2.36(\tilde{\rho}+0.3\tilde{\lambda}^{1/2})}\right]\right\}}\tilde{\lambda}^{-1/4}\,. \qquad (29)$$

The 0.3 terms in this result express the fact that the original derivation of the equation was limited to a plane-stress case with $\nu_{12} = 0.3$.

A much simpler expression, without the limitation of an assumed value for ν_{12}, can be determined from the results given in this paper. It will be observed that the data in Table 3 suggest a linear relationship between $\tilde{\theta}_d^*$ and $\tilde{\rho}$: $\tilde{\theta}_d^* = 3.101 + 2.343\tilde{\rho}$, for $\tilde{H} = 1$ and $1 \leq \tilde{\rho} \leq 5$. From this it is straightforward to use Eqn. 28 to show that

the increase in the effective crack length for a symmetrical DCB is given by

$$a_e/h = (0.258 + 0.195\tilde{\rho})^{1/2}\tilde{\lambda}^{-1/4}. \tag{30}$$

A comparison between this equation and Eqn. 29 shows that the result from Ref. [10] is generally accurate to within 5%, except for very small values of $\tilde{\lambda}$, when the discrepancy is still less than 15%. An expression for the increase in effective crack length in terms of $\tilde{\rho}$ can also be deduced from the empirical results of Suo and co-workers [16]. This result has a discrepancy of no more than 2% for a_e at the largest values of $\tilde{\rho}$, when compared with the present results, corresponding to a slight error in the value of $\tilde{\theta}_d^*$ for a symmetrical DCB that can be calculated from it.

4.1 Compliance of double-cantilever beams

Compliance methods are often used to deduce energy-release rates for DCB geometries. The issues with this for large cohesive-length scales or bridging zones will be discussed elsewhere [28]. However, here we discuss the compliance of a homogeneous DCB with a small cohesive-length scale, so that the usual assumptions of LEFM are met.

Consider a DCB, with arms of equal thickness h and modulus $\bar{E}$, being opened by an applied load P_∞ at a distance a_o from the cohesive crack tip. Assuming a linear system, the total opening displacement at the point where the load is applied is given by

$$\Delta_\infty = \frac{8P_\infty a_o^3}{\bar{E}h^3} + a_o\left(\theta_o^M + \theta_o^{V_d}\right) + u_o^M + u_o^{V_d}\ , \tag{31}$$

where all the terms, except for the last two, have been defined earlier. These last two terms, u_o^M and $u_o^{V_d}$, can be thought of as the contributions to the *root displacement*

from the crack-tip moments and shear forces. The root displacement is the increase in separation between the two centroidal axes at the crack tip (see Fig. 3), and is an analogue to the root rotation.

As with root rotation, the root-displacement is associated with deformation in both the cohesive zone and the arms themselves. It should be noted that the concept of elastic deformation of the arms normal to the interface was invoked by Kanninen's original elastic-foundation model for the DCB geometry [3]. Dimensional considerations show that in a linear system, the crack tip-displacements can be written in the general form

$$\begin{aligned} u_o^M &= \tilde{u}_m M_o / \bar{E}_A h_A \\ u_o^{V_d} &= \tilde{u}_d V_{o_d} / \bar{E}_A \ , \end{aligned} \tag{32}$$

where $\tilde{u}_m$ and $\tilde{u}_d$ are dimensionless constants.

Using Eqns. 18, 23, and 32, and recognizing that $M_o = P_\infty a_o$ and $V_{o_d} = P_\infty$ for a point-loaded DCB, Eqn. 31 can be re-written as

$$\Delta_\infty = \frac{8 P_\infty a_o^3}{\bar{E} h^3} + \frac{P_\infty a_o}{\bar{E} h}\left(\tilde{\theta}_m \frac{a_o}{h} + \tilde{\theta}_d\right) + \frac{P_\infty}{\bar{E}}\left(\tilde{u}_m \frac{a_o}{h} + \tilde{u}_d\right) \ . \tag{33}$$

Since a linear system has been assumed, the energy-release rate is related to the rate of change of compliance with crack length, and one can state that

$$\mathcal{G}_o = -\frac{\partial \Pi}{\partial a_o} = \frac{P_\infty^2}{2}\frac{\partial (\Delta_\infty / P_\infty)}{\partial a_o} = \frac{12 P_\infty^2 a_o^2}{\bar{E} h^3}\left[1 + \frac{\tilde{\theta}_m}{12}\frac{h}{a_o} + \frac{h^2}{24 a_o^2}(\tilde{\theta}_d + \tilde{u}_m)\right] \ . \tag{34}$$

Remembering from Eqn. 24 that $\tilde{\theta}_m = 4\sqrt{3\tilde{\theta}_d}$ for a symmetrical, linear DCB, one can show that $\tilde{u}_m = \tilde{\theta}_d$ is required to make Eqn. 34 identical to Eqn. 28. This result could also have been deduced as a direct consequence of the Maxwell-Betti reciprocal theorem [29]. The shear root-displacement term, $\tilde{u}_d$, does not affect the fracture

mechanics of the DCB geometry.

It should be emphasized that if one assumes there is only a root-rotation at the crack tip, whether this is incorporated as a correction to a clamped Timoshenko beam or not, and neglects the possibility of a root displacement, an inconsistency is introduced between the compliance method and the J-integral method for computing the energy-release rate. Only the root-displacement associated with the crack-tip moment needs to be invoked to rationalize these two concepts. The root-displacement associated with the shear force does not have a role in the relationship between compliance and energy-release rate for a DCB loaded by forces. However, it does have a role in calculations for the wedge test, when the loading parameter is defined by Δ, not P_∞.

4.2 Comparison to an elastic-foundation model

Although not originally cast in those terms, the elastic-foundation model of Kanninen [3] can be viewed as a cohesive-zone model in which the DCB arms have only a bending stiffness, with a linear traction-separation law representing the out-of-plane stiffness of the arms. For an elastic beam of thickness h and modulus $\bar{E}$ supported by linear springs of stiffness k' (per unit area) on a rigid foundation, the root rotations and displacements are given by [29]

$$\theta_o = 2 \times 3^{1/2} \left(\frac{\bar{E}}{hk'} \right)^{1/2} \frac{V_{o_d}}{\bar{E}h} + 4 \times 3^{3/4} \left(\frac{\bar{E}}{hk'} \right)^{1/4} \frac{M_o}{\bar{E}h^2} \tag{35}$$

$$u_o = 2 \times 3^{1/4} \left(\frac{\bar{E}}{hk'} \right)^{3/4} \frac{V_{o_d}}{\bar{E}} + 2 \times 3^{1/2} \left(\frac{\bar{E}}{hk'} \right)^{1/2} \frac{M_o}{\bar{E}h} \tag{36}$$

Such a model represents half of a symmetrical double-cantilever beam geometry, with a spring stiffness of $k = k'/2$. This model does not provide a valid description of the crack-tip stress fields in the small-cohesive-length-scale limit [30]. However, it will be

shown below that, with the use of a single empirical fit, the model correctly describes all the root rotations and displacements in this limit, so it can be used to compute fracture conditions for LEFM. Since there are two identical arms, the root rotations and displacements of a symmetrical DCB are double those given above:

$$\theta_o = 2 \times 6^{1/2} \left(\frac{\bar{E}}{hk}\right)^{1/2} \frac{V_{o_d}}{\bar{E}h} + 4 \times 6^{3/4} \left(\frac{\bar{E}}{hk}\right)^{1/4} \frac{M_o}{\bar{E}h^2} \tag{37}$$

$$u_o = 2 \times 6^{1/4} \left(\frac{\bar{E}}{hk}\right)^{3/4} \frac{V_{o_d}}{\bar{E}} + 2 \times 6^{1/2} \left(\frac{\bar{E}}{hk}\right)^{1/2} \frac{M_o}{\bar{E}h} \; . \tag{38}$$

The corresponding work done against the tractions at the crack tip is

$$\mathcal{W}_o = k u_o^2/2 \; . \tag{39}$$

By comparison to Eqn. 20, it will be seen that the first term on the right hand side of Eqn. 37 is $\theta_o^{V_d}$, and the second term is θ_o^M. Therefore, if $k = 24\bar{E}/\tilde{\theta}_d^2 h$, the first term is identical to the expression for $\theta_o^{V_d}$ given by Eqn. 18. In addition, this identity also makes the second term equivalent to the expression for θ_o^M given by Eqn. 23, with $\tilde{\theta}_m = 4\sqrt{3\tilde{\theta}_d}$ (as shown at the beginning of Section 4). Furthermore, with $M_o = P_\infty a_o$ and $V_{o_d} = P_\infty$, substitution of Eqn. 38 into Eqn. 39 results in Eqn. 28. Finally, a comparison between the equations for the root-displacement (Eqns. 38 and 32) confirms the observation that $\tilde{u}_m = \tilde{\theta}_d$. It also indicates that $\tilde{u}_d = \tilde{\theta}_d^{3/2}/(2\sqrt{3})$, which is a new result that could not be obtained by the analyses of the earlier sections.

In Kanninen's original formulation [3], k was identified with the average transverse stiffness of the arms, so it was assumed to be given by $k = \bar{E}/h$. This corresponds to the approximation that $\tilde{\theta}_d = \sqrt{24}$, and it can be verified from the equations given in this paper that it gives a reasonably good approximation for the energy-release rate under LEFM conditions. For example, Eqn. 28 shows that this approximation

gives a value of $0.64h$ for the fictitious increase in crack length needed to correct for shear effects in effective crack models [3, 25], rather than the correct value of $0.673h$. The correct value for $\tilde{\theta}_d$ under LEFM conditions and for a symmetrical DCB is 5.44 (Table 1). This corresponds to a spring stiffness of $k = 0.811\bar{E}/h$ [17]. Substituting this value into Eqns. 37 and 38, Eqn. 33 can be used to show that the compliance for a DCB is

$$\frac{\Delta_\infty}{P_\infty} = \frac{24}{\bar{E}}\left[\frac{a_o^3}{3h^3} + \left(\frac{\tilde{\theta}_d}{12}\right)^{1/2}\frac{a_o^2}{h^2} + \left(\frac{\tilde{\theta}_d}{12}\right)\frac{a_o}{h} + 0.5\left(\frac{\tilde{\theta}_d}{12}\right)^{3/2}\right] . \tag{40}$$

The specific result for an isotropic DCB is given by setting $\tilde{\theta}_d$ to 5.44:

$$\frac{\Delta_\infty}{P_\infty} = \frac{1}{\bar{E}}\left[8\frac{a_o^3}{h^3} + 16.2\frac{a_o^2}{h^2} + 10.9\frac{a_o}{h} + 3.66\right] . \tag{41}$$

This provides a minor correction to the equivalent result given in Ref. [3].

The elastic foundation model can also be used for an orthotropic system. Using Eqn. 25, and remembering that $\bar{E} = \bar{E}_{11}$ and $\tilde{\lambda} = \bar{E}_{22}/\bar{E}_{11}$, it can be readily seen that $k = 24\bar{E}_{22}/\tilde{\theta}_d^{*^2}h$. All the results for a symmetrical DCB are then rigorously reproduced by the elastic-foundation model. The root displacements are

$$\begin{aligned} u_o^M &= \tilde{\theta}_d^* \frac{M_o}{\bar{E}_{11}^{1/2}\bar{E}_{22}^{1/2}h} \\ u_o^{V_d} &= \frac{\tilde{\theta}_d^{*3/2}}{2\sqrt{3}}\frac{V_o}{\bar{E}_{11}^{1/4}\bar{E}_{22}^{3/4}} , \end{aligned} \tag{42}$$

and the compliance of an orthotropic DCB is given by Eqn. 40 as

$$\frac{\Delta_\infty}{P_\infty} = \frac{24}{\bar{E}_{11}}\left[\frac{a_o^3}{3h^3} + \left(\frac{\tilde{\theta}_d^*}{12\sqrt{\tilde{\lambda}}}\right)^{1/2}\frac{a_o^2}{h^2} + \left(\frac{\tilde{\theta}_d^*}{12\sqrt{\tilde{\lambda}}}\right)\frac{a_o}{h} + 0.5\left(\frac{\tilde{\theta}_d^*}{12\sqrt{\tilde{\lambda}}}\right)^{3/2}\right] . \tag{43}$$

5 Conclusions

We have followed the work of Andrews and Massabò [12] to demonstrate how the concept of root-rotation is linked to phase angles and to the energy-release rate associated with shear in a beam-like geometry. However, we have developed a simpler approach in which shear deformation does not need to be separated from root rotations, and simple-beam theory can be used without resorting to Timoshenko-beam theory.

The contribution to the energy-release rate from transverse shear forces is simply the product of the shear force and the associated root rotation at the crack tip. This is valid, not only in the LEFM limit, but also for adhesive bonds with large-scale cohesive lengths, and for composites with large-scale bridging. It has been shown that this approach is completely consistent with earlier analyses of the effect of shear [17, 12]. However, a new concept that arises from the present approach is the need to consider root displacements at a crack tip to ensure consistency between root-rotation and compliance-based calculations of energy-release rates.

For the special case of a symmetrical DCB, we have demonstrated how this approach is tightly linked to the elastic-foundation model of Kanninen [3]. One empirical fitting parameter is required to provide complete consistency between this model and later, rigorous approaches used to model the effects of shear on a symmetrical DCB.

Acknowledgements

The author gratefully acknowledges many hours of discussions with Prof. Bent F. Sørensen, and the detailed comments that were provided on several iterations of the

manuscript. The author also acknolwedges the Otto Mønsted foundation for a Guest Professorship at the Wind Energy Department at DTU Risø campus, and support from the Janine Johnson Weins Endowed Professorship Fund at the University of Michigan. He also thanks Dr. Lars P. Mikkelsen and his family for their generous hospitality during visits to Risø.

References

[1] P. P. Gillis and J. J. Gilman. Double-cantilever cleavage mode of crack propagation. *Journal of Applied Physics*, 35:647–658, 1964.

[2] S. Mostovoy, P. B. Crosley and E. J. Ripling. Use of crack-line-loaded specimens for measuring plane-strain fracture toughness. *Journal of Materials*, 2:661–681, 1967.

[3] M. F. Kanninen. Augmented double cantilever beam model for studying crack propagation and arrest. *International Journal of Fracture*, 9:83–92, 1973.

[4] B.F. Sørensen, A. Horsewell, O. Jørgensen, A.N. Kumar and P. Engbæk. Fracture resistance measurement method for in situ observation of crack mechanisms. *Journal of the American Ceramic Society*, 81:661–669, 1998.

[5] B. F. Sørensen, K. Jørgensen, T. K. Jacobsen and R. C. Østergaard. DCB-specimen loaded with uneven bending moments. *International Journal of Fracture*, 141:163–176, 2006.

[6] British Standard. *Determination of the mode I adhesive fracture energy G_{IC} of structure adhesives using the double cantilever beam (DCB) and tapered double cantilever beam (TDCB) specimens*, BS 7991:2001 edition.

[7] ASTM. *Standard Test Method for Fracture Strength in Cleavage of Adhesives in Bonded Metal Joints*, D3433-99 (2012) edition.

[8] J. R. Barber. *Elasticity*. Springer, Dordrecht, The Netherlands, 2010.

[9] R. B. Sills and M. D. Thouless. Cohesive-length scales for damage and toughening mechanisms,. *International Journal of Solids and Structures*, 55:32–43, 2015.

[10] J. G. Williams. End corrections for orthotropic DCB specimens. *Journal of Composite Science and Technology*, 35:367–376, 1989.

[11] ASTM. *Standard Test Method for Mode I Interlaminar Fracture Toughness of Unidirectional Fiber-Reinforced Polymer Matrix Composites*, D5528-13 (2013) edition.

[12] M. G. Andrews and R. Massabò. The effects of shear and near tip deformations on energy release rate and mode mixity of edge-cracked orthotropic layers. *Engineering Fracture Mechanics*, 74:2700–2720, 2007.

[13] C. T. Sun and R. K. Pandey. Improved method for calculating strain energy release rate based on beam theory. *AIAA Journal*, 32:184–189, 1994.

[14] J. Wang and P. Qiao. Mechanics of bimaterial interface: Shear deformable split bilayer beam theory and fracture. *Journal of Applied Mechanics*, 72:674–682, 2005.

[15] S. M. Wiederhorn, A. M. Shorband and R. L. Moses. Critical analysis of the theory of the double cantilever method of measuring fracture surface energy. *Journal of Applied Physics*, 39:1569–1572, 1968.

[16] Z. Suo, G. Bao, B. Fan and T. C. Wang. Orthotropy rescaling and implications for fracture in composites. *International Journal of Solids and Structures*, 28:235–248, 1991.

[17] S. Li, J. Wang and M. D. Thouless. The effects of shear on delamination of beam-like geometries. *Journal of the Mechanics and Physics of Solids*, 52:193–214, 2004.

[18] Z. Suo and J. W. Hutchinson. Interface crack between two elastic layers. *International Journal of Fracture*, 43:1–18, 1990.

[19] J. P. Parmigiani and M. D. Thouless. The effects of cohesive strength and toughness on mixed-mode delamination of beam-like geometries. *Engineering Fracture Mechanics*, 74:2675–2699, 2007.

[20] R. B. Sills and M. D. Thouless. The effect of cohesive-law parameters on mixed-mode fracture. *Engineering Fracture Mechanics*, 109:353–368, 2013.

[21] J. Dundurs. Edge-bonded dissimilar orthogonal elastic wedges. *Journal of Applied Mechanics*, 36:650–652, 1969.

[22] Z. Suo. Delamination specimens for orthotropic materials. *Journal of Applied Mechanics*, 57:627–634, 1990.

[23] A. J. Paris and P. C. Paris. Instantaneous evaluation of J and C^*. *International Journal of Fracture*, 38:R19–R21, 1988.

[24] P. Olsson and U. Stigh. On the determination of the constitutive properties of thin interphase layers - an exact solution. *International Journal of Fracture*, 41:R71–R76, 1989.

[25] J. G. Williams. Large displacement and end block effects in the DCB interlaminar test in modes I and II. *Journal of Composite Materials*, 21:330–347, 1987.

[26] B. F. Sørensen and T. K. Jacobsen. Crack growth in composites: Applicability of R-curves and bridging. *Plastics, Rubber and Composites*, 29:119–133, 2000.

[27] G. Bao, S. Ho, Z. Suo and B. Fan. The role of material orthotropy in fracture specimens for composites. *International Journal of Solids and Structures*, 29:11051116, 1992.

[28] M. D. Thouless and B. F. Sørensen. On the use of the compliance method for analyzing large-scale bridging problems. *Manuscript in preparation*, 2017.

[29] J. R. Barber. *Intermediate Mechanics of Materials*. Springer, Dordrecht, The Netherlands, 2011.

[30] H. Wang, W. Lu, J. R. Barber and M. D. Thouless. The roles of cohesive strength and toughness for crack growth in visco-elastic and creeping materials. *Engineering Fracture Mechanics*, 160:226–237, 2016.

$\tilde{H}_B$ \ $\tilde{\alpha}_B$	-0.8	-0.6	-0.4	-0.2	0	0.2	0.4	0.6	0.8
0.0	2.69	2.86	3.10	3.39	3.76	4.37	5.24	6.81	10.8
0.2	2.67	2.85	3.07	3.36	3.76	4.36	5.29	7.04	11.6
0.4	2.71	2.92	3.18	3.54	4.04	4.78	5.95	8.21	14.4
0.6	2.77	3.02	3.37	3.82	4.44	5.36	6.86	9.77	18.1
0.8	2.84	3.17	3.60	4.15	4.92	6.05	7.89	11.5	22.1
1.0	2.92	3.35	3.87	4.52	5.44	6.79	9.03	13.4	26.3

Table 1: Values of $\tilde{\theta}_d$ for isotropic bi-layers, with $\tilde{\beta} = 0$ [17].

$\tilde{H}_B$ \ $\tilde{\alpha}_B$	-0.8	-0.6	-0.4	-0.2	0	0.2	0.4	0.6	0.8
0.0	5.35	5.72	6.20	6.75	7.42	8.35	9.54	11.4	15.1
0.2	5.40	5.88	6.44	7.09	7.89	8.94	10.3	12.6	17.1
0.4	5.62	6.30	7.08	7.96	9.07	10.5	12.5	15.7	23.0
0.6	5.96	6.95	8.04	9.31	10.8	12.8	15.7	20.6	32.7
0.8	6.43	7.83	9.35	11.1	13.2	16.0	20.1	27.3	46.1
1.0	7.03	8.96	11.0	13.3	16.2	20.0	25.7	35.9	63.2

Table 2: Values of $\tilde{\theta}_m$ for isotropic bi-layers, with $\tilde{\beta} = 0$, calculated from Ref. [17].

$\tilde{H}$ \ $\tilde{\rho}$	1	3	5
0.0	3.81	6.43	8.93
0.2	3.77	6.68	9.54
0.4	4.04	7.37	10.66
0.6	4.44	8.21	11.96
0.8	4.91	9.15	13.36
1.0	5.44	10.14	14.81

Table 3: Values of $\tilde{\theta}_d^*$ for homogeneous orthotropic layers, calculated from Ref. [12]. These values are accurate for $0.025 \leq \tilde{\lambda} \leq 1$ [12].

$\tilde{H}$ \ $\tilde{\rho}$	1	3	5
0.0	7.44	10.05	12.03
0.2	7.90	10.71	12.88
0.4	9.07	12.35	14.89
0.6	10.85	14.80	17.87
0.8	13.21	18.04	21.80
1.0	16.15	22.06	26.66

Table 4: Values of $\tilde{\theta}_m^*$ for homogeneous orthotropic layers, calculated from Ref. [12]. These values are accurate for $0.025 \leq \tilde{\lambda} \leq 1$ [12].

$\tilde{H}$ \ $\tilde{\rho}$	1	3	5
0.0	1°	-2°	-3°
0.2	-0.7°	-2°	-3°
0.4	-0.8°	-2°	-2°
0.6	-0.6°	-1°	-1°
0.8	-0.4°	-1°	-1°
1.0	0°	0°	0°

Table 5: Values of $\psi_o^{V_d}$ for orthotropic layers, calculated from Eqn. 24. The phase angles for $\tilde{\rho} \neq 1$ have been rounded, to reflect the uncertainty associated with the very small dependency of ψ_o^M on $\tilde{\rho}$.

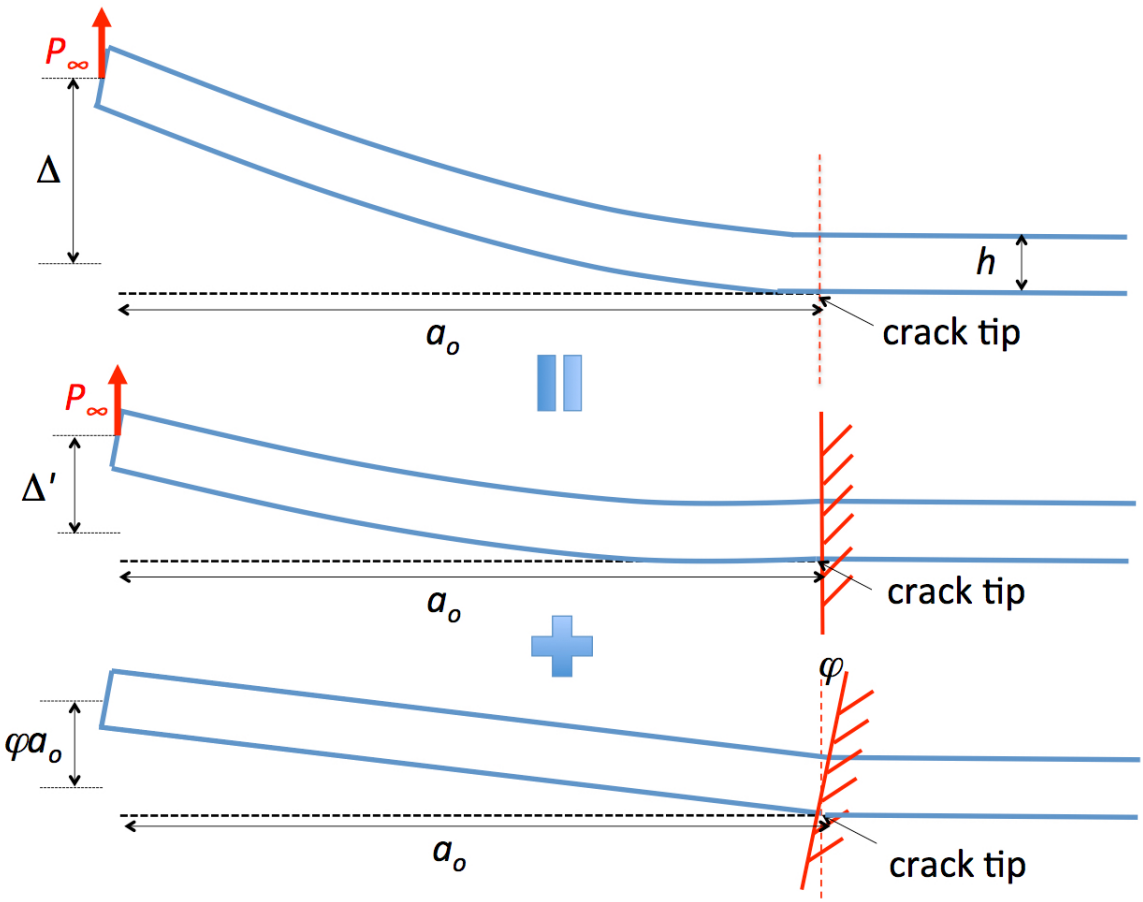

Figure 1: The crack-mouth opening, Δ of a beam that forms part of a double-cantilever beam with a crack length of a_o (top), can be considered to be made up of two contributions: $\Delta' = 4P_\infty a_o^3/Eh^3 + P_\infty a_o/\kappa_s Gh$, representing the deflection of a clamped Timoshenko beam (middle), and φa_o, representing the rotation of the clamped boundary (bottom).

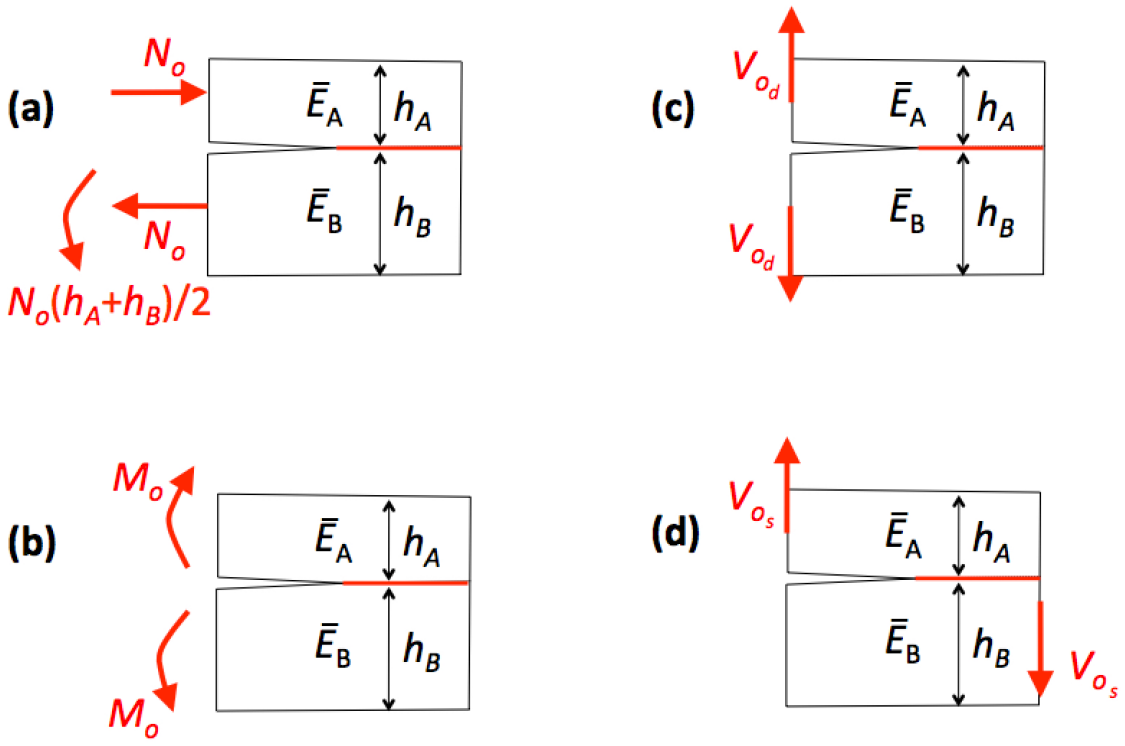

Figure 2: The basic crack-tip loads for which interfacial fracture mechanics solutions exist: **(a)** axial loads, **(b)** moments, **(c)** symmetrical shear forces acting at the crack and **(d)** a single shear force at the crack tip. The energy-release rates for (a) and (b) are given by general solutions that have no dependence on the nature of the cohesive tractions along the interface. Conversely, the energy-release rates for (c) and (d) depend on the cohesive-length scale of the tractions. Note that the shear forces in (d) are taken to be those immediately ahead and behind the crack tip, with the separation between them being vanishingly small, so no compensating moment has been drawn on the figure.

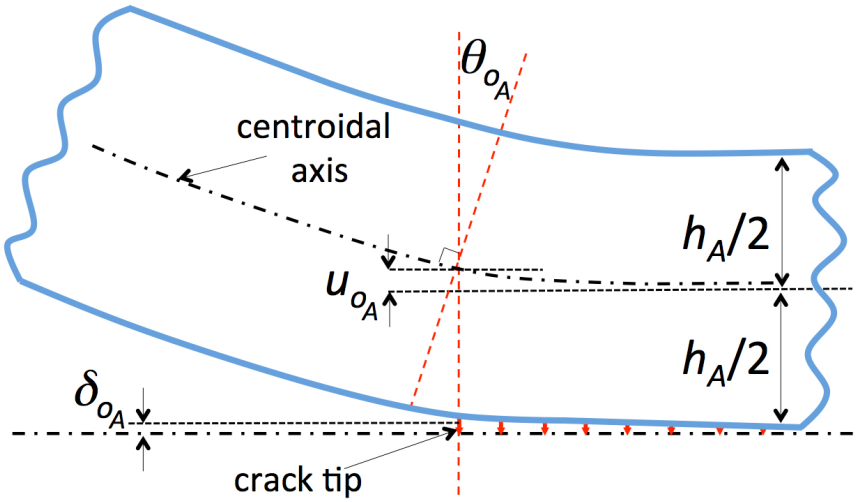

Figure 3: A schematic diagram of the tip of an interface crack showing how the centroidal axis of the section rotates at the crack tip - coupling both the effects of shear and root rotation into a single parameter. The usual approach of imposing a rotation on a clamped boundary of a Timoshenko beam, would result in a kink in the angle at the crack tip. This figure shows that the smooth slope assumed here, must also be accompanied by a root-displacement, u_{o_A}, which is discussed in a subsequent section. This root displacement has one contribution from the separation of the interface, δ_{o_A}, and a second contribution from the elastic deformation of the arms.

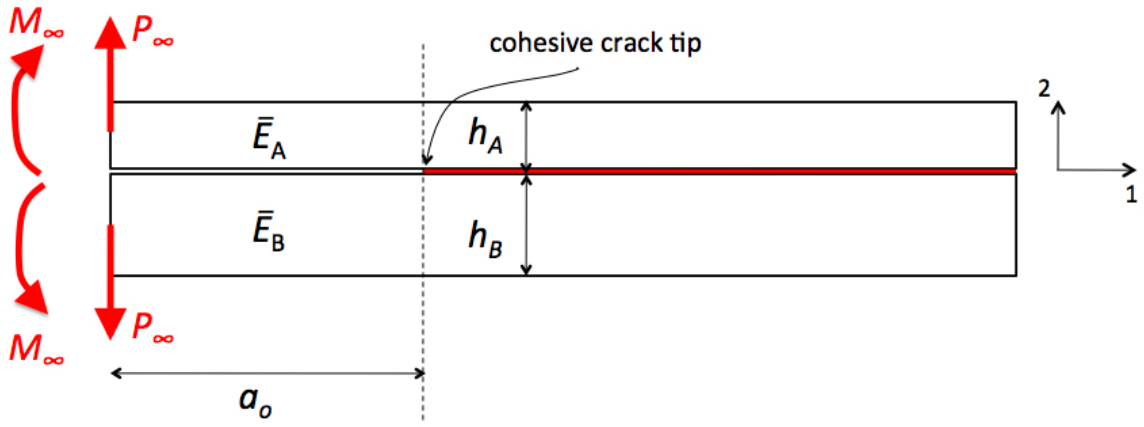

Figure 4: A general double-cantilever-beam geometry with applied moment, M_∞, and load, P_∞, a crack length a_o, arm thicknesses h_A and h_B, and elastic moduli, $\bar{E}_A$ and $\bar{E}_B$.

Appendix: Asymmetrical shear

An analysis similar to that described in the main text can be repeated for geometries in which a shear force is applied to only one arm. Consider such a geometry shown in Fig. A-1, in which a force of P_∞ is applied to one arm at a distance a_o behind the crack tip, along with a moment applied to both arms. There are different ways in which the moments can be applied to maintain equilibrium. However, to simplify the analysis, we have chosen to distribute the moments by assigning a reference value of M_∞ to the bottom arm, and a corresponding moment $M^* = M_\infty - P_\infty a_o$ to the top arm. A corresponding force, P_∞, and moment, $P_\infty L$, are applied at a distance L ahead of the crack to maintain equilibrium (Fig. A-1). This particular loading configuration has been chosen so that the crack-tip loads and moments are described by superposition of the basic cases illustrated in Fig. 2(b) and (d).

Evaluating the J-integral around an external contour of the geometry shown in Fig, A-1 gives the result

$$J_{ext} = P_\infty \Theta_A + \frac{6M^{*2}}{\bar{E}_A h_A^3} + \frac{6M_\infty^2}{\bar{E}_B h_B^3} - \frac{P_\infty^2 L^2}{2\bar{E}_c I_C} \tag{A-1}$$

where $\bar{E}_c I_C$ is the bending stiffness of the uncracked segment C, ahead of the crack, and the angle Θ_A is the total rotation between the line of action of the force applied to the upper arm and the line of action of the force applied to the segment ahead of the crack.

The rotation, Θ_A, has contributions from (i) θ_{o_A}, the root rotation of the top arm relative to the bonded interface, (ii) the deformation of the upper arm behind the

crack tip, and (iii) the deformation of the uncracked ligament ahead of the crack:

$$\Theta_A = \theta_{o_A} + \frac{6P_\infty a_o^2}{\bar{E}_A h_A^3} + \frac{12M^* a_o}{\bar{E}_A h_A^3} - \frac{P_\infty L^2}{2\bar{E}_c I_C} + \frac{P_\infty L^2}{\bar{E}_c I_C} \ . \tag{A-2}$$

As before, the effect of shear deformation of the beams is being incorporated into the root rotation, so there is no need for a Timoshenko-beam analysis.

Substituting the equation for Θ_A into Eqn. A-1, and using the fact that $M^* = M_\infty - P_\infty a_o$, one obtains

$$J_{ext} = P_\infty \theta_{o_A} + \frac{6M_\infty^2}{\bar{E}_A h_A^3}\left[\tilde{\Sigma}\tilde{H}^3 + 1\right] = \mathcal{G}_o = \mathcal{W}_o \tag{A-3}$$

The result for only an asymmetrical shear at the crack tip is generated by the special case of $M_\infty = 0$, so that $M^* = -P_\infty a_o$. Then, by recognizing that the shear force at the crack tip is given by $V_{o_s} = P_\infty$, one obtains a general equation for $\mathcal{W}_o^{V_s}$:

$$\mathcal{W}_o^{V_s} = V_{o_s}\theta_{o_A}^{V_s} \ , \tag{A-4}$$

where $\theta_{o_A}^{V_s}$ is the root rotation, associated with shear only, of the top arm relative to the bonded interface.

For a linear system, the root rotation associated with shear must be given by

$$\theta_{o_A}^{V_s} = \tilde{\theta}_{s_A} V_{o_s}/\bar{E}_A h_A \ , \tag{A-5}$$

so that

$$\mathcal{W}_o^{V_s} = \tilde{\theta}_{s_A} V_{o_s}^2/\bar{E}_A h_A \ . \tag{A-6}$$

This is identical to the form given in Ref. [17] for the energy-release rate corresponding to asymmetrical shear (Fig. 2d).

In a linear system with a combined moment, M_o, and shear force, $V_o^{V_s}$, acting at the crack tip, the root rotation is

$$\theta_{o_A} = \theta_{o_A}^{M} + \theta_{o_A}^{V_s} \ , \tag{A-7}$$

where $\theta_{o_A}^{M}$ is the root rotation of the top arm in response to a crack-tip moment only:

$$\theta_{o_A}^{M} = \tilde{\theta}_{m_A} M_o / \bar{E}_A h_A^2 \ . \tag{A-8}$$

Following the same argument that was used to derive Eqn. 22 in Section 3.1, it can be shown that the crack-tip phase angle for asymmetrical shear, $\psi_o^{V_s}$ is given by

$$\cos\left(\psi_o^{M} - \psi_o^{V_s}\right) = \tilde{\theta}_{m_A} \left[24\tilde{\theta}_{s_A}(\tilde{\Sigma}\tilde{H}^3 + 1)\right]^{-1/2} \ . \tag{A-9}$$

Numerical values for the energy-release rate associated with a asymmetrical shear force, $\mathcal{G}_o^{V_s}$, and the corresponding crack-tip phase angle, $\psi_o^{V_s}$, are given in Ref. [17] for the limiting case of LEFM. These can be used to deduce values for $\tilde{\theta}_{s_A}$ and $\tilde{\theta}_{m_A}$, which are reproduced in Tables A-1 and A-2. Corresponding values for orthotropic materials can be deduced from Ref. [12], recognizing from that reference that

$$\begin{aligned} \tilde{\theta}_{s_A} &= \tilde{\theta}_{s_A}^{*}(\tilde{H}, \tilde{\rho})\tilde{\lambda}^{-1/2} \\ \tilde{\theta}_{m_A} &= \tilde{\theta}_{m_A}^{*}(\tilde{H}, \tilde{\rho})\tilde{\lambda}^{-1/4} \ , \end{aligned} \tag{A-10}$$

and

$$\tilde{\theta}_{s_A}^{*} = \left[\tilde{b}_{s_A} + \frac{\tilde{\rho}}{\kappa_s(1+\tilde{H})}\right] \ , \tag{A-11}$$

with $\kappa_s = 5/6$, and the values of $\tilde{b}_{s_A}$ given in Table 1 of Ref. [12]. The values of $\tilde{\theta}_{s_A}^{*}$ and $\tilde{\theta}_{m_A}^{*}$ are reproduced in Tables A-3 and A-4. Where they can be directly compared, the values for these two parameters calculated from Refs. [17] and [12] differ only by minor numerical discrepancies.

As with symmetrical shear, the results can also be expressed in terms of the energy-release rate, $\mathcal{G}_o^{V_s}$ and phase angle $\psi_o^{V_s}$. These can be found directly in Ref. [17] for isotropic materials. The phase angle, $\psi_o^{V_d}$, for orthotropic materials can be calculated from Eqn. A-9 using the root rotations presented above, and assuming that ψ_o^M is given by the isotropic values. The results are presented in Table A-5.

$\tilde{H}$ \ $\tilde{\alpha}$	-0.8	-0.6	-0.4	-0.2	0	0.2	0.4	0.6	0.8
0.0	2.69	2.86	3.10	3.39	3.76	4.37	5.24	6.81	10.8
0.2	2.58	2.65	2.76	2.94	3.21	3.62	4.31	5.66	9.33
0.4	2.34	2.27	2.28	2.39	2.62	2.99	3.64	4.90	8.13
0.6	2.00	1.83	1.83	1.92	2.13	2.47	3.05	4.09	6.34
0.8	1.64	1.45	1.45	1.56	1.75	2.06	2.53	3.28	4.57
1.0	1.32	1.16	1.18	1.28	1.46	1.71	2.07	2.58	3.19

Table A-1: Values of $\tilde{\theta}_{s_A}$ for isotropic layers with $\tilde{\beta} = 0$ [17].

$\tilde{H}$ \ $\tilde{\alpha}$	-0.8	-0.6	-0.4	-0.2	0	0.2	0.4	0.6	0.8
0.0	5.35	5.72	6.20	6.75	7.42	8.35	9.54	11.4	15.1
0.2	5.34	5.75	6.23	6.81	7.53	8.44	9.68	11.6	15.5
0.4	5.35	5.78	6.28	6.89	7.68	8.65	9.99	12.1	16.3
0.6	5.30	5.76	6.31	6.97	7.81	8.87	10.3	12.5	16.8
0.8	5.26	5.72	6.32	7.05	7.95	9.08	10.6	12.8	16.9
1.0	5.17	5.68	6.35	7.13	8.07	9.27	10.8	13.1	16.8

Table A-2: Values of $\tilde{\theta}_{m_A}$ for isotropic layers,with $\tilde{\beta} = 0$, calculated from Ref. [17].

$\tilde{H}$ \ $\tilde{\rho}$	1	3	5
0.0	3.81	6.42	8.93
0.2	3.21	5.68	8.10
0.4	2.62	4.77	6.90
0.6	2.13	3.97	5.78
0.8	1.75	3.31	4.85
1.0	1.46	2.78	4.09

Table A-3: Values of $\tilde{\theta}^*_{s_A}$ for orthotropic layers, calculated from Ref. [12]. These values are accurate for $0.025 \leq \tilde{\lambda} \leq 1$ [12].

$\tilde{H}$ \ $\tilde{\rho}$	1	3	5
0.0	7.44	10.05	12.03
0.2	7.53	10.23	12.31
0.4	7.67	10.49	12.66
0.6	7.82	10.71	12.95
0.8	7.95	10.88	13.16
1.0	8.08	11.03	13.33

Table A-4: Values of $\tilde{\theta}^*_{m_A}$ for orthotropic layers, calculated from Ref. [12]. These values are accurate for $0.025 \leq \tilde{\lambda} \leq 1$ [12].

$\tilde{H}$ \ $\tilde{\rho}$	1	3	5
0.0	1°	-2°	-3°
0.2	-3.5°	-6°	-6°
0.4	-7.4°	-9°	-10°
0.6	-10.4°	-12°	-13°
0.8	-13.1°	-15°	-16°
1.0	-15.1°	-17.2°	-18.0°

Table A-5: Values of $\psi_o^{V_s}$ for orthotropic layers, calculated from Eqn. A-9. The phase angles have been rounded, except for $\tilde{\rho} = 1$ and $\tilde{H} = 1$, to reflect the uncertainty associated with the very small dependency of ψ_o^M on $\tilde{\rho}$.

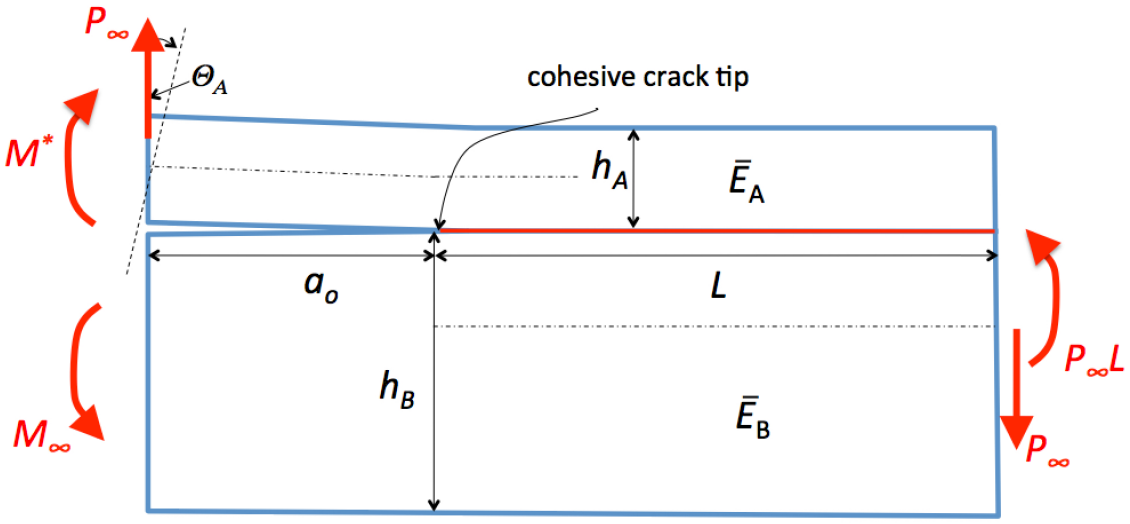

Figure A-1: A laminated structure loaded by a force P_∞ applied to only one arm, and a bending moment M_∞. Equilibrium, requires that $M^* = M_\infty - P_\infty a_o$.